

# Two-Dimensional Segmentation to Reconstruct Three-Dimensional Covid-19 Patient's Lung CT Using Active Contour

Zaki Ambadar

Department of Biomedical Engineering  
Institut Teknologi Sepuluh Nopember  
Surabaya, Indonesia 60111  
zakai.ambadar@gmail.com

Tri Arief Sardjono

Department of Biomedical Engineering  
Institut Teknologi Sepuluh Nopember  
Surabaya, Indonesia 60111  
sardjono@bme.its.ac.id

Nada Fitriyatul Hikmah

Department of Biomedical Engineering  
Institut Teknologi Sepuluh Nopember  
Surabaya, Indonesia 60111  
nadafh@its.ac.id

**Abstract**—Beginning in December 2019, SARS-CoV-2, also referred to as COVID-19, quickly spread over the world. With two recurrent waves and a 3.3% fatality rate, COVID-19 has caused over 4 million cases in Indonesia. RT-PCR, antigen, and RT-LAMP are currently the main techniques for COVID-19 detection and diagnosis. A CT scan is usually used for additional diagnosis when RT-PCR results are uncertain, but extra confirmation is required. The need to inform patients about the effects of COVID-19 on the lungs is increasing as the number of cases of the virus keeps rising and diagnosis and first aid techniques advance. The severity of COVID-19-induced pneumonia, which shows up as ground-glass opacities (GGO), which are gray patches in the lung cavity, may be seen on a single-slice CT scan. The degree of lung injury can be measured using image processing techniques. In this study, two- and three-dimensional representations of the lungs were created utilizing a multi-slice CT scan and image processing techniques like active contour and marching cubes. The suggested approach produced an average volume difference of 5% and an accuracy of 62% based on intersection over union (IoU).

**Keywords**—3D Visualization, Active Contour, Marching Cubes, Binary Thresholding, COVID-19

## I. INTRODUCTION

COVID-19, caused by the SARS-CoV-2 virus that first appeared in December 2019, has proven to be a severe illness responsible for millions of deaths globally, and continues to pose significant health risks for those recovering from it [1]. Coronaviruses originated in animals like bats and transmitted to other animals before reaching humans [2]. COVID-19 also attacked the country of Indonesia and had a high impact with a total case of over 4 million with a mortality rate of 3.3% [3]. The number of COVID-19 cases in doubled during two major waves. The disease was peaking on January 30, 2021 with 14,518 new cases and on July 18, 2021 with 44,721 new cases [4]. According to WHO, the symptoms of COVID-19 patients are dry cough, fever, fatigue, and loss of sensitivity of the senses of taste and smell. More severe symptoms include difficulty in breathing, loss of cognitive movement and body mobility, confusion, and chest pain [5].

There are several methods available for detecting COVID-19 in patients. The virus can be identified through PCR (Polymerase Chain Reaction) tests, Lateral Flow Tests (LFTs), and antibody tests [6]. Current diagnostic methods for

COVID-19 include reverse-transcription polymerase chain reaction (RT-PCR), real-time RT-PCR, and reverse transcription loop-mediated isothermal amplification (RT-LAMP) [7]. RT-LAMP, known for its high specificity, offers sensitivity comparable to RT-PCR, and has been effective in detecting MERS-CoV. Typically, RT-PCR is used to diagnose patients showing COVID-19 symptoms, but for cases that are difficult to detect, other diagnostic tools, such as CT scans, can be employed [8].

For a more detailed evaluation of COVID-19 patients, further diagnostic testing can be performed using medical imaging techniques. These include modalities such as CT (Computed Tomography), MRI (Magnetic Resonance Imaging), Ultrasound, X-ray, and Nuclear Medicine Imaging, including Positron Emission Tomography (PET) [9]. CT imaging provides higher clarity compared to X-rays as it uses a rotating light source [9]. CT scans help eliminate the need for exploratory surgery [9]. In COVID-19 patients CT scans often show gray or white patches in the lungs referred to as ground-glass opacity (GGO) as well as other abnormalities such as enlarged blood vessels, bilateral irregularities, lower lobe involvement, and posterior predilection [10]. To utilize CT scan images effectively an image processing step called segmentation is required.

Segmentation is the process of dividing an image into regions with similar properties, such as gray level, color, texture, brightness, and contrast [11]. The purpose of segmentation is to separate an object in an image. In medical imaging, segmentation is used to study anatomical structures, locate tumors or lesions, calculate tumor volume, and assist in patient treatment planning. Segmentation methods include amplitude thresholding, edge detection, active contours, and region-based techniques [11].

Segmentation can be applied to both two-dimensional and three-dimensional images such as those from PET scans, MRI, and CT scan. Three-dimensional segmentation involves stacking two-dimensional images and reconstructing them in three-dimensional space which allows for visualization and quantification of the scanned subjects [12]. It is possible to observe the organs and tissues of COVID-19 patients using CT scan, allowing for an evaluation of lung damage. CT scan images demonstrate various patterns of lung damage caused by COVID-19, which can be categorized into four main types.

The first category, known as Typical Appearance, is characterized by peripheral and bilateral ground-glass opacities (GGO) accompanied by intralobular lines, commonly referred to as crazy paving. The second category, Indeterminate Appearance, lacks the typical features but presents with multifocal, diffuse, perihilar, or unilateral GGO, with or without consolidation. The third category, Atypical Appearance, is distinguished by the absence of typical or indeterminate features, displaying consolidation without GGO. Lastly, the category Negative for pneumonia refers to cases where there are no CT features indicative of pneumonia, such as typical, indeterminate, or atypical appearances.

The appearance of COVID-19 on chest CT images follows a somewhat predictable pattern over time [13]. Asymptomatic patients with SARS-CoV-2 often have normal chest CT results and some symptomatic patients may also show normal findings. Moreover, lung abnormalities on chest CT are not specific to COVID-19 [13]. Owing to these limitations, chest CT should not be used independently to diagnose or rule out COVID-19. RT-PCR test results remain the diagnostic standard and a critical part of clinical decision-making [13].

Further identification of COVID-19 features in CT scans may be necessary and this is where segmentation and reconstruction come into play. Segmentation is done with the main objective of isolating a part that you want to focus on from other parts like separating lung images from elements such as the heart, ribs, and skin, and to isolate GGO nodules from the lungs [14]. High accuracy (94.6%), sensitivity (90.2%), and specificity (95.9%) were achieved using an active shape model. Segmentation by Sri Widodo demonstrate how segmentation separates specific elements for further analysis [14].

The marching cubes algorithm can be used to visualize segmentation results in three dimensions. In a study by Shuaibu Ali Gombe, the ITK/VTK/QT framework was used for lung segmentation and visualization in order to enhance lung cancer diagnosis accuracy by segmenting and visualizing lung tissue in three dimensions. Ali Gombe used a region-based segmentation technique to separate lung structures from other components like the ribs and heart. The marching cubes algorithm then applied for 3D visualization. Ali Gombe recommended exploring other segmentation techniques for improved results such as automatic and semi-automatic methods [15].

The aim of this study is to develop an algorithm capable of segmenting lung tissue from CT thorax images, isolating ground-glass opacity (GGO) regions, and creating a 3D model that can be visualized using any 3D software or printed with a 3D printer. By utilizing an active contour model created by Chan-Vese and binary segmentation, it is theoretically possible to generate a lung and GGO nodule segmentation mask and use marching cubes to create a 3D model of the infected lung volume.

## II. PROPOSED METHOD

As seen in Figure 1, the system suggested in this study consists of multiple steps. After being extracted from the Harvard Dataverse, the DICOM images undergo a pre-processing step. Finding the foreground and background objects, contrast stretching, adaptive histogram equalization, and non-linear filtering are all part of the pre-processing step. To distinguish the lung regions from other structures including the ribs, spine, skin, and tissues, the segmentation step uses

active contour modeling, threshold-based segmentation, and morphological processes. The marching cubes algorithm, picture orientation, and STL output file creation are all part of the three-dimensional reconstruction step. This makes it possible to turn the segmented data into a three-dimensional model that can be printed out and used for interactive point cloud plot viewing.

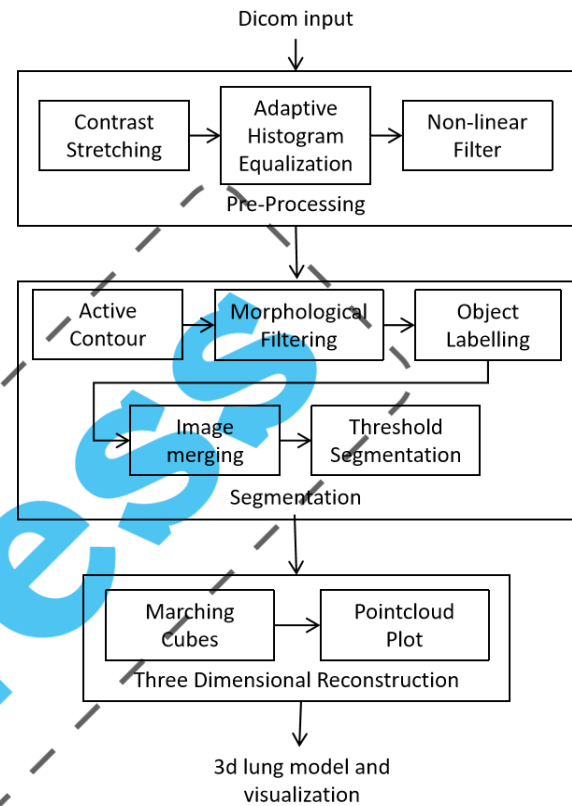


Fig. 1. Flowchart Diagram of Research.

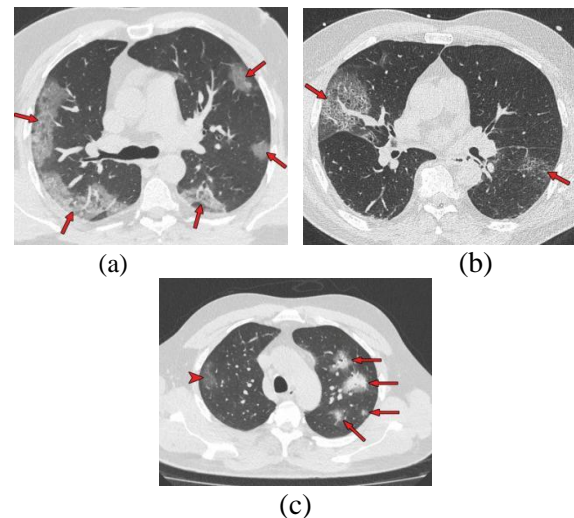


Fig. 2. (a) Ground-Glass Opacity in a Peripheral Distribution, (b) Crazy-Paving Pattern Highlighted, (c) Consolidation Surrounded by Ground-Glass Opacities [13].

### A. Data

The dataset utilized in this study consists of three subjects exhibiting characteristic manifestations of COVID-19. These include ground-glass opacity with a peripheral distribution, as illustrated in Figure 2(a), a crazy-paving pattern, as depicted

in Figure 2(b), and consolidation surrounded by ground-glass opacities, as shown in Figure 2(c). The inclusion of subjects with confirmed COVID-19-related lung damage is essential, as the primary objective of this research is to detect and analyze the extent of lung damage caused by the virus, rather than merely identifying the infection status.

### B. Pre-processing

Pre-processed DICOM files were obtained from the Harvard Dataverse [16], an open-access repository. RT-PCR was used to confirm that every individual in this repository tested positive for COVID-19. The pre-processing phase concentrates on improving the DICOM pictures to attain the best possible segmentation circumstances, which call for distinct sharpness and grayscale value distinction. This was accomplished by applying a non-linear filter, contrast stretching, and adaptive histogram equalization.

#### 1) Contrast Stretching

Choosing the ideal histogram range is essential for segmentation. The distribution of the histogram is equalized using adaptive histogram equalization (AHE), but the range of the histogram is not increased. Contrast stretching improves the image's intensity values by expanding the histogram range [17].

#### 2) Adaptive Histogram Equalization

Low contrast is a common problem with images, making them less usable. Adaptive Histogram Equalization (AHE) improves contrast by evaluating the image's cumulative distribution function (CDF) and modifying the histogram, which enhances darker sections while minimizing too bright spots.

#### 3) Non-linear Filter

A non-linear filter is used to remove noise and interference present in the CT scan images. The image will be subjected to a median filter is used to remove speckle noise and salt-and-pepper noise which are the common artifacts in CT scans that can reduce the accuracy level and damage the segmentation results.

#### 4) Segmentation

Segmentation is the main component of this system. It involves isolating the region of interest (in this case, the lungs and visible ground-glass opacities) from other anatomical structures. The segmentation process is divided into three stages: binary segmentation, active contour modeling, and morphological operations.

#### 5) Active Contour

Active contour modeling is employed to remove skin, bones, heart, and others as well as isolate the lungs from internal organs. The active contour used in this study is the Chan-Vese model, also known as the active contour without edges (ACWE). Chan-Vese's active contour algorithm is derived from the segmentation problem formulated by Mumford and Shah. Edge detectors are used, in classic active contour and snake models depending on image gradients, to stop curves at the desired object boundary from expanding. On the other hand, the duration of the active Chan-Vese contour termination is independent of the image gradient [18][19]. The Chan-Vese method depends on minimizing segmentation-based energy, with the initial contours of this method using a checkerboard pattern [20].

#### 6) Threshold Segmentation

Threshold-based segmentation is performed to isolate ground-glass opacities within the lung region. If this step were performed before lung isolation, other tissues with similar grayscale values to the opacities might also be segmented and complicating the process. This segmentation is done by setting a boundary from a white-black value of an image and the value that is behind a boundary will be removed and made black, while the value that prioritizes the boundary will be set and made white. This segmentation will give mask results from GGO on the lungs of COVID-19 patients

#### 7) Morphological Operation

Morphological operations, such as dilation and erosion, are conducted to finalize the segmentation process. These operations address imperfections such as unknown nodules or segmented noise by refining the results. The output is a binary image prepared for three-dimensional reconstruction.

### C. 3D Reconstruction Process

After the segmentation process is complete, the next step is visualization and three-dimensional reconstruction. This process employs two primary methods which are volume-based modeling using Lewiner's marching cubes algorithm and point cloud plotting. The point cloud method is utilized due to the large amount of data so it allows for an initial interactive view before performing a volume reconstruction. Marching Cubes is an algorithm used to reconstruct from a binary image and plot the three-dimensional information in three-dimensional space. This binary image is an array with binary numbers that can be processed by the marching cube to reconstruct it according to the dimensions of the per-slice image [21]. Marching cubes uses the points of each array an array in two dimension as vertices to create a face, and then uses the surrounding points above or below in the three dimensional space to create a voxel. The result of this reconstruction is a three-dimensional view of the image that can be seen in Figure 3.

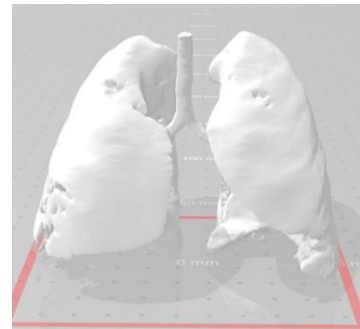


Fig. 3. 3D Reconstruction Using Marching Cubes

### D. Data Analysis

The reconstructed data will be analyzed using 3D Slicer software. Volumetric analysis and visualization will be conducted through the Lung CT Analyzer project. Lung segmentation can be performed either by placing a few manual markers on the lung or by using a deep learning-based lung and lobe segmentation algorithm. The software also supports a sensitive, manually assisted growcut method for airway segmentation. The Lung Analyzer identifies five regions of interest using thresholding and grow-from-seed techniques: bulla/emphysema, inflated, infiltrated, collapsed, and lung vessel. The volume of each segment is calculated through segment statistics. The results are overlaid onto 2D

views using standard color codes: black for bulla, blue for inflated, yellow for infiltrated, pink for collapsed, and red for vessels. In addition, 3D spatial reconstructions of the affected lung segments are available for further analysis.

### E. Data Validation Process

The data will be evaluated using a confusion matrix to assess the accuracy of the segmentation. The ground truth for the segmentation results will be established using another application, specifically 3D Slicer, which will serve as the primary reference. The confusion matrix will allow for the comparison of two segmentation outcomes: one produced using the proposed research method and the other using the 3D Slicer method. True positive (TP), true negative (TN), false positive (FP), and false negative (FN) findings will be examined in order to assess how well the two approaches compare. FP denotes cases identified by the proposed method but not by the reference method, FN denotes cases that the proposed method misses but are detected by the reference method, TP denotes cases accurately detected by both methods, and TN involves cases where neither method detects the condition. Table 1 provides the confusion matrix.

TABLE I. CONFUSION MATRIX

		True Values	
		TRUE	FALSE
Prediction	TRUE	<i>True Positive</i>	<i>False Positive</i>
	FALSE	<i>False Negative</i>	<i>True Negative</i>

Key performance metrics will be calculated to evaluate the overall effectiveness of the proposed method. These metrics provide a comprehensive assessment of how well the segmentation approach identifies the true regions of interest and minimizes errors. Table 2 presents these metrics which derived from the confusion matrix values enabling a clearer understanding of the method's reliability compared to the reference segmentation.

TABLE II. FORMULAS FOR CONFUSION MATRIX

Metric	Formula	Definition
Accuracy	$\frac{TP + TN}{TP + FP + FN + TN}$	Proportion of observations that are true
Sensitivity	$\frac{TP}{TP + FN}$	Proportion of positive cases that were predicted to be correct
Specificity	$\frac{TN}{TN + FP}$	Proportion of true predictive negative cases

## III. EXPERIMENTAL RESULTS

This chapter presents the results derived from the methodology outlined in the previous chapter. The study includes three subjects, with data obtained from the Harvard Dataverse, as depicted in Figure 4. Subject ID 94028 is illustrated in Figure 4(a), subject ID 13758 is presented in Figure 4(b), and subject ID 22052 is highlighted in Figure 4(c).

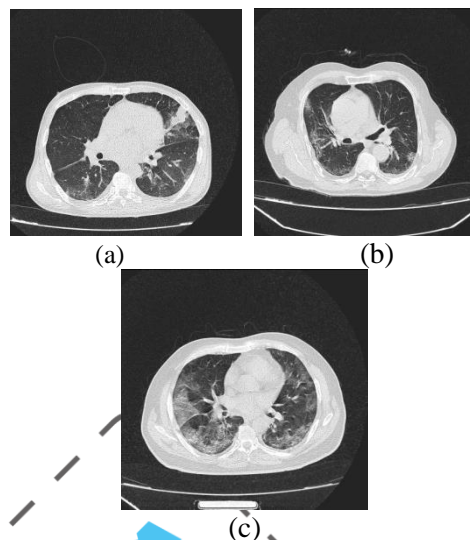


Fig. 4. The subjects used in this research: subject ID 94028 (a), subject ID 13758 (b), and subject ID 22052 (c), all accessible via the Harvard Dataverse.

The lung images exhibit typical characteristics of COVID-19 with the existence of ground-glass opacities for most part and consolidation as seen in Figure 4(a) in the right lobe. The crazy-paving pattern is visible in the left lobe as shown in Figure 4(b). Given these observations this study will proceed with these subjects. Contrast stretching was applied to enhance and redistribute the intensity values in the histogram, as illustrated in Table 3. This technique highlighted the ground-glass opacities (GGO) and the crazy-paving pattern which are crucial for detection. To equalize the histogram with the lung volume, encompassing the diseased and healthy parts, adaptive histogram equalization (AHE) was utilized. Additionally, it decreased noise; a higher PSNR denoted higher-quality images. Following these preparation processes, pictures were prepared for the ACWE algorithm's segmentation.

After the contrast correction stage, the image still has noise and artifacts that come with the CT Scan modality. This stage is also to make the segmentation algorithm easier to identify the edges of the lungs, body, and air using the median filter. This step will produce an image with a clearer lung content because all parts of the lung that differ slightly in pixels will merge into one color that is more similar as shown in Table 3, the kernel used is 5x5 because the kernel gives the highest PSNR value compared to 3x3 and 7x7, and in the 3x3 kernel there is still a little noise that has not been seen, and the 7x7 kernel begins to remove details and information from the image.

The ACWE is used for segmentation. This morphological active contour uses a checkerboard pattern as the initialization of the contour, and each iteration will shrink following the edge of the existing image, where in this image is the edge of the body cavity and the body itself. The more iteration the ACWE has, the better the result will be. In Figure 5, after the 29th iteration there are no more changes in the image, but we keep it in the range of 35 as the other subjects might need more iteration in order to get the best result.

The infected lung image is obtained by the segmentation using the hounsfield window between -600 hounsfield units and window width of 1500 hounsfield units [24][25][26]. These values were used to filter the histogram, retaining only the data between the white values of -600 and 1500.

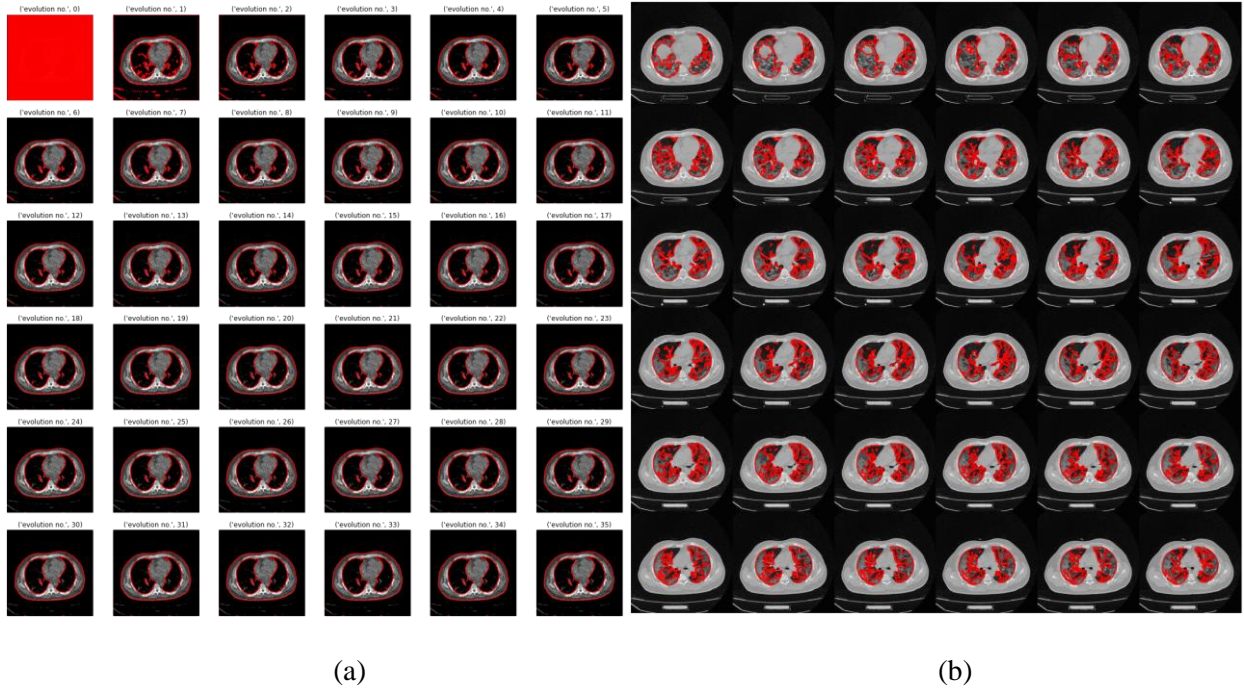
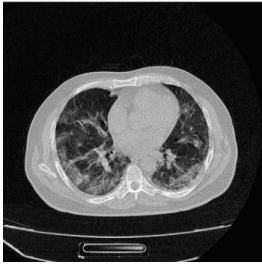
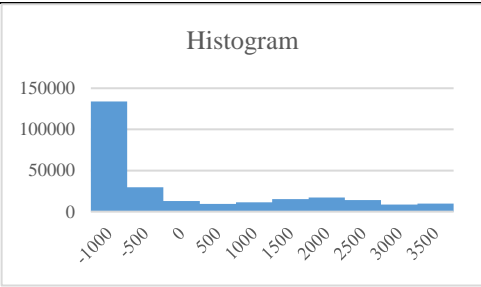

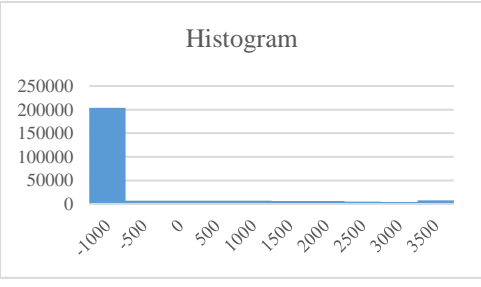


Fig 5. Evolution of segmentation using ACWE (a) and the final segmentation result using the ACWE mask (b)

TABLE III. CONTRAST STRETCHING AND ADAPTIVE HISTOGRAM EQUALIZATION RESULTS

No.	Image	Histogram	PSNR
1.	<p>contrast stretching</p> 	<p>Histogram</p> 	8.42
2.	<p>adaptive equalization + contrast stretching</p> 	<p>Histogram</p> 	38.32

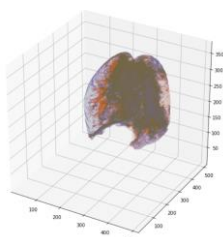
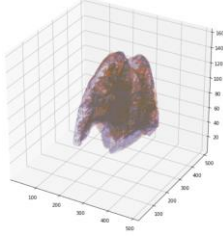
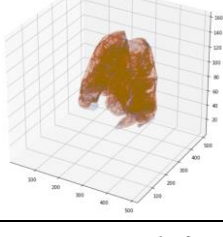
After this process, morphological filtering was repeated. As shown in Figure 5, some lung vessels were mistakenly segmented as part of the infected lung, though this is also evident in the ground truth, indicating a marginal error in the automatic segmentation process for COVID-19-affected lungs. The segmented images were used to reconstruct a 3D model of each lung using Lewiner's marching cubes algorithm for volumetric rendering, and point cloud plotting for a lighter, interactive 3D view of the lungs. Both methods successfully visualized the infected portions of the lung, marked in yellow, while the uninfected areas were marked in blue. The results were validated using the confusion matrix method and intersection over union, with comparisons made to

groundtruth obtained via 3D Slicer using the LungCTAnalyzer and LungCTSegmenter tools. COVID-19 masking results were extracted, and comparisons were performed.

As seen in Table 4, the first patient had a relatively high accuracy but a much lower similarity index of 42%. This is due to the presence of tissue in the right lobe with similar white levels to other body tissues, making it challenging for the active contour algorithm to differentiate between lung and non-lung tissue. The other patients had similarity index values of 67.8% and 77.4%, indicating that their segmentation results were closer to the actual lung margins and infected regions, as

their lungs did not exhibit a high concentration of similarly dense tissues. The confusion matrix results show a higher accuracy due to the calculation of black pixels in the image. If the image is used in its original dimensions, the abundance of black pixels can inflate the accuracy. To mitigate this, the images were cropped using bounding boxes around the lungs, minimizing the presence of black pixels that could artificially increase the accuracy value. As a result, the cropped dimensions for patient ID 94028 were 300, 270, and 350; for patient ID 13758, 140, 230, and 280; and for patient ID 22052, 153, 280, and 340, where the first number represents the number of slices, the second the length, and the third the height. A physical 3D-printed model was additionally created for each subject, with representations provided in Figure 6. The model for patient ID 94028 is depicted in Figure 6(a), followed by the model for patient ID 13758 in Figure 6(b), and the model for patient ID 22052 in Figure 6(c).

TABLE IV. DATA VALIDATION USING CONFUSION MATRIX AND INTERSECTION OVER UNION

No	3d model visualization	Confusion Matrix	Intersection Over Union
1		Accuracy = 0.9245 Specificity = 0.9413 Sensitivity = 0.9158	0.42485410 976746185
2		Accuracy = 0.962 Specificity = 0.80 Sensitivity = 0.980	0.67907145 0577287
3		Accuracy = 0.969 Specificity = 0.986 Sensitivity = 0.8529	0.77478241 14302613

#### IV. CONCLUSION

Using the active contour method, this work suggests a system for two-dimensional segmentation and three-dimensional reconstruction for the display of lung CT scan images of COVID-19 patients. 3D Slicer software was used to validate the data, which came from the Harvard Dataverse archive. The outcome of this study is a three-dimensional reconstruction of lung models from COVID-19 patients, each with distinct markings. The images of patients with IDs 94028, 13758, and 22052 achieved confusion matrix accuracy values of 92%, 96%, and 97%, respectively, and intersection over union similarity indices of 42%, 67%, and 77%. The models created using the marching cubes algorithm can be 3D-printed for direct visualization, while the point cloud plot provides a rough visualization of the damaged lung areas. This

visualization can assist patients in understanding the condition of their lungs.

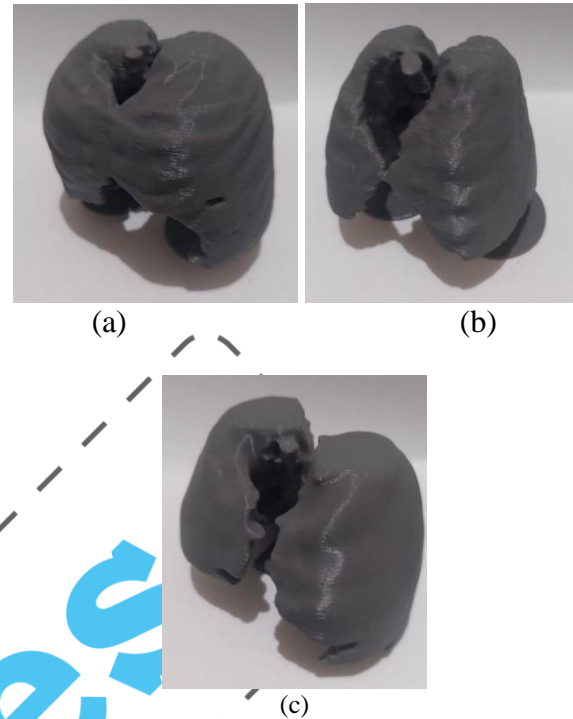


Fig. 6. 3D printed lung model of subject ID 94028 (a), subject ID 13758 (b), and subject ID 22052 (c).

#### REFERENCES

- [1] R. Dharma, S. Khan, R. Tiwari, et al., "Coronavirus disease 2019–COVID-19," *Clin. Microbiol. Rev.*, vol. 33, no. 4, pp. e00028–20, Jun. 2020, doi: 10.1128/CMR.00028-20.
- [2] S. Chaplin, "COVID-19: a brief history and treatments in development," *Prescriber*, vol. 31, pp. 23–28, 2020, doi: 10.1002/psb.1843.
- [3] "Coronavirus Cases," [Online]. Available: <https://www.worldometers.info/coronavirus/country/indonesia/>. [Accessed: Sep. 27, 2021].
- [4] E. Dong, H. Du, and L. Gardner, "An interactive web-based dashboard to track COVID-19 in real time," *The Lancet Infect. Dis.*, vol. 20, no. 5, pp. 533–534, 2020.
- [5] "Coronavirus," [Online]. Available: [https://www.who.int/health-topics/coronavirus#tab=tab\\_3](https://www.who.int/health-topics/coronavirus#tab=tab_3). [Accessed: Dec. 14, 2021].
- [6] D. Jarrom, L. Elston, J. Washington, et al., "Effectiveness of tests to detect the presence of SARS-CoV-2 virus, and antibodies to SARS-CoV-2, to inform COVID-19 diagnosis: a rapid systematic review," *BMJ Evid.-Based Med.*, vol. 27, pp. 33–45, 2022.
- [7] P. Zhai, Y. Ding, X. Wu, J. Long, Y. Zhong, and Y. Li, "The epidemiology, diagnosis and treatment of COVID-19," *Int. J. Antimicrob. Agents*, vol. 55, no. 5, 2020.
- [8] S. Salehi, A. Abedi, S. Balakrishnan, and A. Gholamrezanezhad, "Coronavirus disease 2019 (COVID-19): A systematic review of imaging findings in 919 patients," *Am. J. Roentgenol.*, vol. 215, no. 1, pp. 87–93, 2020.
- [9] Z. Hughes, "Medical imaging types and modalities," [Online]. Available: <https://www.ausmed.com/cpd/articles/medical-imaging-types-and-modalities>. [Accessed: Dec. 14, 2021].
- [10] T. C. Kwee and R. M. Kwee, "Chest CT in COVID-19: What the radiologist needs to know," *Radiographics*, vol. 40, no. 7, pp. 1848–1865, 2020.
- [11] N. Sharma and L. M. Aggarwal, "Automated medical image segmentation techniques," *J. Med. Phys.*, vol. 35, no. 1, p. 3, 2010.
- [12] "What is 3D Image Segmentation and How Does It Work?," [Online]. Available: <https://www.synopsys.com/glossary/what-is-3d-image-segmentation.html>. [Accessed: Dec. 14, 2021].

- [13] T. C. Kwee and R. M. Kwee, "Chest CT in COVID-19: What the radiologist needs to know," *Radiographics*, vol. 40, no. 7, pp. 1848–1865, 2020.
- [14] S. Widodo and Wijayanto, "Lung field segmentation on computed tomography," *Kursor J.*, pp. 99–108, 2013.
- [15] S. A. Gombe, "3D visualization and segmentation of lungs using ITK/VTK/Qt framework," Master's Thesis, Tallinn Univ. Technol. Sch. Inf. Technol., 2017.
- [16] S. M. Mostafavi, "COVID19-CT-Dataset: An open-access chest CT image repository of 1000+ patients with confirmed COVID-19 diagnosis," *Harvard Dataverse*, V1, 2021, doi: 10.7910/DVN/6ACUZI.
- [17] K. Firdausy, T. Sutikno, and E. Prasetyo, "Image enhancement using contrast stretching on RGB and IHS digital image," *TELKOMNIKA (Telecommun. Comput. Electron. Control.)*, vol. 5, p. 45, 2007, doi: 10.12928/telkomnika.v5i1.1335.
- [18] T. Chan and L. Vese, "An active contour model without edges," in *Scale-Space Theories in Computer Vision*, M. Nielsen, P. Johansen, O. F. Olsen, and J. Weickert, Eds. Berlin, Heidelberg: Springer, 1999, vol. 1682, pp. 141–151, doi: 10.1007/3-540-48236-9\_13.
- [19] P. Getreuer, "Chan-Vese segmentation," *Image Process. On Line*, vol. 2, pp. 214–224, 2012.
- [20] K. H. Rahouma, S. M. Mabrouk, and M. Aouf, "Lung cancer diagnosis based on Chan-Vese active contour and polynomial neural network," *Procedia Comput. Sci.*, vol. 194, pp. 22–31, 2021.
- [21] K. A. Mandaliana, T. Harsono, and R. Sigit, "3D visualization and reconstruction of lung cancer images using marching cubes algorithm," in *2019 Int. Electron. Symp. (IES)*, 2019, pp. 143–147, doi: 10.1109/ELECSYM.2019.8901667.
- [22] R. Bumm, A. Lasso, N. Kawel-Böhm, A. Wäckerlin, P. Ludwig, and M. Furrer, "First results of spatial reconstruction and quantification of COVID-19 chest CT infiltrates using lung CT analyzer and 3D slicer," *Br. J. Surg.*, vol. 108, Suppl. 4, May 2021, doi: 10.1093/bjs/znab202.077.
- [23] E. Lanza, R. Muglia, I. Bolengo, et al., "Quantitative chest CT analysis in COVID-19 to predict the need for oxygenation support and intubation," *Eur. Radiol.*, vol. 30, no. 12, pp. 6770–6778, 2020, doi: 10.1007/s00330-020-07013-2.
- [24] K. Li, Y. Fang, W. Li, et al., "CT image visual quantitative evaluation and clinical classification of coronavirus disease (COVID-19)," *Eur. Radiol.*, vol. 30, no. 8, pp. 4407–4416, 2020, doi: 10.1007/s00330-020-06817-6.
- [25] C. S. Guan, Z. B. Lv, S. Yan, et al., "Imaging features of coronavirus disease 2019 (COVID-19): Evaluation on thin-section CT," *Acad. Radiol.*, vol. 27, no. 5, pp. 609–613, 2020, doi: 10.1016/j.acra.2020.03.002.
- [26] W. Lu, J. Wei, T. Xu, et al., "Quantitative CT for detecting COVID-19 pneumonia in suspected cases," *BMC Infect. Dis.*, vol. 21, no. 836, 2021, doi: 10.1186/s12879-021-06556-z.

In Press